Error in unsaturated stochastic models parameterized with field data

Robert M. Holt

Department of Geology and Geological Engineering, University of Mississippi, University, Mississippi, USA

John L. Wilson

Department of Earth and Environmental Science, New Mexico Institute of Mining and Technology, Socorro, New Mexico, USA

Robert J. Glass

Flow Visualization and Processes Laboratory, Sandia National Laboratories, Albuquerque, New Mexico, USA

Received 23 March 2001; revised 14 May 2002; accepted 24 May 2002; published 8 February 2003.

[1] We use Monte Carlo error analysis to illustrate the impact of measurement errors in field-estimated hydraulic properties on predictions made with 1D and 3D unconditional stochastic models of unsaturated flow and transport. Monte Carlo simulations are conducted across a series of simplified artificial realities completely described by the Gardner–Russo parametric model. The mean values of properties are varied between simulations to elucidate the relationship between true properties and prediction errors. Hydraulic properties are reestimated by simulating tension infiltrometer measurements in the presence of small simple errors. Two types of observation error are considered, along with one inversion-model error resulting from poor contact between the instrument and the medium. Errors in the spatial statistics of hydraulic properties cause critical stochastic model assumptions to be violated, limiting the usable parameter space for model predictions. Even where critical assumptions are valid, stochastic model predictions show significant error, and the magnitude and pattern of error changes with the true property means, the flow conditions, and the type of measurement error. Mean velocities may show errors up to an order of magnitude. The velocity variance is overestimated by up to three orders of magnitude during 3D flow and eight orders of magnitude during 1D flow. The 1D velocity integral scale is underestimated by as much as five orders of magnitude. The estimates for 1D longitudinal macrodispersivity are surprisingly robust and show relatively small error across most of the parameter space. *INDEX TERMS:* 1869 Stochastic processes; 1875 Unsaturated zone; 1829 Groundwater hydrology; 1832 Groundwater transport; *KEYWORDS:* stochastic models, unsaturated zone, geostatistics, spatial bias, measurement error, inversion model error

Citation: Holt, R. M., J. L. Wilson, and R. J. Glass, Error in unsaturated stochastic models parameterized with field data, *Water Resour. Res.*, *39*(2), 1028, doi:10.1029/2001WR000544, 2003.

1. Introduction

[2] Predictive stochastic flow and transport models are parameterized with the spatial statistics of measured, or estimated, hydraulic properties. The accuracy of predictions depends on the accuracy of input spatial statistics and ultimately the accuracy of the property estimates used to determine these statistics. Errors in property estimates are difficult to quantify and are often unknown because the physics of property measurements are highly complex and variable. A single property estimate can be affected by a combination of errors in simple observations and inversion-model errors, including errors in governing equations, boundary conditions, initial conditions, and constitutive relationships. The type and magnitude of these errors may vary spatially, with the true properties of the sampled medium, and temporally, with the sampling conditions. Simple uncorrelated random errors affecting measurements of hydraulic properties can cause a large systematic distortion, or bias, in spatial statistics determined from property data [*Holt*, 2000; *Holt et al.*, 2002]. When biased spatial statistics are used to parameterize stochastic models of flow and transport, stochastic model predictions will also show systematic error. The extent and nature of this error has not been previously investigated.

[3] In this paper, we use error analysis techniques to explore the relationship between errors in field-estimated unsaturated hydraulic properties and stochastic model predications for unsaturated flow and transport and to illustrate some consequences of using field-estimated property data to parameterize predictive stochastic models. We conduct Monte Carlo error analyses across a series of simplified artificial realities, where constitutive relationships are completely known. We vary the mean values of hydraulic properties between realities to elucidate the connection between the

0043-1397/03/2001WR000544$09.00

true properties and bias in stochastic model predictions. Because it is virtually impossible to develop a complete set of error models for measurement of unsaturated hydraulic properties, we choose to conduct our error analyses with a limited number of property measurement errors.

[4] Our procedure is straightforward. For each artificial reality, we generate spatially correlated random fields of properties and estimate the properties using simulated field measurements subject to known random errors. We then determine the spatial statistics of both the true and estimated properties and use these statistics to parameterize stochastic models. We then assess the errors in these stochastic model predictions. The procedure is repeated for all realities to illustrate the sensitivity of prediction errors to the true spatial statistics and the type of measurement error affecting property estimates.

[5] In all of our realities, we assume that Richard's equation is valid and that unsaturated hydraulic properties are completely described by the Gardner–Russo [*Gardner*, 1958; *Russo*, 1988] parametric model. We also assume that the log saturated hydraulic conductivity and the *Gardner* [1958] parameter are normally distributed second-order stationary random functions completely characterized by their mean, variance and an exponential covariance function. For convenience, we assume that the Gardner–Russo tortuosity parameter is equal to zero. No specified cross correlation between parameters is assumed. All property estimates result from simulated tension infiltrometer measurements, a simple field device for estimating both the hydraulic conductivity and the *Gardner* [1958] parameter. We assume that measurements are made under steady state conditions and that subsample-scale heterogeneity does not exist. To minimize the degrees of freedom in our problem, we allow only two types of observation error (transducer errors) to affect property estimates, along with one inversion-model (boundary condition) error resulting from poor contact between the instrument and the medium. In the absence of errors, tension infiltrometer measurements return error-free estimates of spatial statistics for the hydraulic conductivity and the *Gardner* [1958] parameter. All locations in a reality are sampled to eliminate errors in spatial statistics due to nonideal sampling locations, thereby insuring that bias in spatial statistics and stochastic model predictions reflects only property measurement errors.

[6] We use two different unconditional stochastic models for this analysis, each representing end-members in the style of heterogeneity. The first is based on the seminal work of *Yeh et al.* [1985a, 1985b], where it is assumed that hydraulic parameters are statistically isotropic. The second model is that of *Zhang et al.* [1998], where the hydraulic parameters are perfectly layered. Geologic materials lie between these two extremes, with most materials showing distinct layering. These two models are consistent with the parametric models used in our assumed realities.

[7] We evaluate errors for several stochastic model predictions, specifically estimates of the mean, variance, and integral scale of the fluid velocity and the longitudinal macrodispersivity. We focus on the ensemble statistics for the velocity, because velocity fields or moments are required input for contaminant transport calculations. The mean velocity is inversely proportional to mean travel time. The ensemble velocity variance measures the point variability in velocity over all possible realizations and is, therefore, a metric for the uncertainty in travel time over short travel distances. The integral scale of the velocity is a measure of the continuity of the ensemble flow field. The longitudinal macrodispersivity can be related to the uncertainty in mean travel times, especially over large travel distances.

2. Theoretical Background

[8] For calculating the mean, variance, and integral scale of velocity and the longitudinal macrodispersivity, we modify steady flow stochastic models presented by *Yeh et al.* [1985a, 1985b] and by *Zhang et al.* [1998]. We extend the work of *Yeh et al.* [1985a, 1985b] and derive a mean and variance of the velocity for 3D unsaturated flow through statistically isotropic media under mean unit-gradient conditions with spatially varying effective moisture content. *Zhang et al.* [1998] developed models for unit-gradient flow through perfectly stratified media (1D flow), including expressions for the mean and variance of velocity. For the model of Zhang et al., we derive additional expressions for the velocity integral scale and the longitudinal macrodispersivity. We review critical components of these models and their extensions below.

[9] These steady flow models satisfy continuity

$$\nabla \cdot \mathbf{q}(\mathbf{x}) = 0 \tag{1}$$

and Darcy's law

$$q_i(\mathbf{x}) = -K(\mathbf{x})\left[-\frac{\partial h(\mathbf{x})}{\partial x_i} - \delta_{i1}\right] \tag{2}$$

where $\mathbf{q}$ is the specific discharge vector, $h(\mathbf{x})$ is the absolute value of the tension head, $K(\mathbf{x})$ is the unsaturated hydraulic conductivity scalar which is a random space function, and $\delta_{i1} = 1$ when i equals 1, representing the vertical direction, and $\delta_{i1} = 0$ otherwise. We assume that $K(\mathbf{x})$ is lognormally distributed and that $Y(\mathbf{x}) = \ln[K(\mathbf{x})]$, which may be decomposed into a mean and perturbation, $Y(\mathbf{x}) = \langle Y(\mathbf{x})\rangle + Y'(\mathbf{x})$. Similarly, we have $q_i(\mathbf{x}) = \langle q_i(\mathbf{x})\rangle + q_i'(\mathbf{x})$ and $h(\mathbf{x}) = \langle h(\mathbf{x})\rangle + h'(\mathbf{x})$, and (2) can be rewritten as

$$\langle q_i(\mathbf{x})\rangle + q_i'(\mathbf{x}) = K^G(\mathbf{x})\left[1 + Y'(\mathbf{x}) + \frac{Y'^2}{2} + \ldots\right] \cdot \left[\frac{\partial\langle h(\mathbf{x})\rangle}{\partial x_i} + \frac{\partial h'(\mathbf{x})}{\partial x_i} + \delta_{i1}\right] \tag{3}$$

where $K^G(\mathbf{x}) = \exp[\langle Y(\mathbf{x})\rangle]$ is the geometric mean of $K(\mathbf{x})$. Taking the expected value of (3) and retaining terms up to first order gives

$$\langle q_i(\mathbf{x})\rangle = K^G(\mathbf{x}) J_i(\mathbf{x}) \tag{4}$$

where $J_i(\mathbf{x}) = (\partial\langle h(x)\rangle/\partial x_i) + \delta_{i1}$ is the mean hydraulic gradient in the direction x_i. Following the approach taken for most stochastic models [e.g., *Yeh et al.*, 1985a, 1985b; *Russo*, 1993, 1995; *Harter and Yeh*, 1996; *Yang et al.*, 1996; *Zhang et al.*, 1998], we assume that flow is dominated by gravity and that $J_i(\mathbf{x}) = \delta_{i1}$. Subtracting (4) from (3) and retaining terms up to first order yields

$$q_i'(\mathbf{x}) = K^G[\, j_i(\mathbf{x}) + \delta_{i1} Y'(\mathbf{x})] \tag{5}$$

where $j_i(\mathbf{x}) = -\delta h'(\mathbf{x})/\partial x_i$ is the perturbation in the gradient. The single point covariance of the specific discharge $\sigma^2_{q_{ij}} = \langle q_i'(\mathbf{x}) q_j'(\mathbf{x})\rangle$ is

$$\sigma^2_{q_{ij}} = K^{G^2}\left[\sigma^2_{j_{ji}} + \delta_{i1}\ \sigma^2_{Y'j_i} + \delta_{j1}\ \sigma^2_{Y'j_j} + \delta_{i1}\delta_{j1}\sigma^2_{Y'}\right] \tag{6}$$

where $\sigma^2_{j_{ij}}$ is the single point covariance of the gradient in the i and j directions, $\sigma^2_{Y'j_i}$ is the single point covariance between $Y'(\mathbf{x})$ and $j_i(\mathbf{x})$, and $\sigma^2_{Y'}$ is the variance of $Y'(\mathbf{x})$. The seepage velocity, u_i is related to the specific discharge, q_i, by

$$u_i(\mathbf{x}) = \frac{q_i(\mathbf{x})}{\theta_e(\mathbf{x})} \tag{7}$$

where $\theta_e = \theta - \theta_{im}$ is the effective volumetric moisture content, θ is the volumetric moisture content, and θ_{im} is the immobile moisture content. We follow *Zhang et al.* [1998] and assume that immobile moisture does not affect advective transport. With $\theta_e = \langle\theta_e\rangle + \theta_e'$, the velocity (7) can be written as

$$u_i(\mathbf{x}) = \frac{\langle q_i\rangle + q_i'(\mathbf{x})}{\langle\theta_e\rangle}\left[1 - \frac{\theta_e'(\mathbf{x})}{\langle\theta_e\rangle} + \frac{\theta_e'^2(\mathbf{x})}{\langle\theta_e\rangle^2} + \cdots\right] \tag{8}$$

To the first order, the mean velocity is

$$\langle u_i\rangle = \frac{\langle q_i\rangle}{\langle\theta_e\rangle}, \tag{9}$$

the perturbation in velocity is

$$u_i'(\mathbf{x}) = \frac{q_i'(\mathbf{x})}{\langle\theta_e\rangle} - \frac{\langle q_i\rangle\theta_e'(\mathbf{x})}{\langle\theta_e\rangle^2}, \tag{10}$$

and the variance of the velocity is

$$\sigma^2_{u_{ij}} = \frac{1}{\langle\theta_e\rangle^2}\left(\sigma^2_{q_{ij}} - \langle u_i\rangle\sigma^2_{q_j\theta_e} - \langle u_j\rangle\sigma^2_{q_i\theta_e} + \langle u_i\rangle\langle u_j\rangle\sigma^2_{\theta_e}\right), \tag{11}$$

where $\sigma^2_{q_i\theta_e}$ is the single point covariance between the specific discharge, q_i, and the effective moisture content, θ_e, and $\sigma^2_{\theta_e}$ is the variance of the effective moisture content. In deriving (9), it is assumed that $\sigma^2_{\theta_e}/\langle\theta_e\rangle^2$ is small ($\ll$1).

[10] In order to derive the statistical moments required for parameterizing (9) and (11), we must specify constitutive models for K and θ_e as functions of tension h. Because of its mathematical simplicity, the Gardner–Russo [*Gardner*, 1958; *Russo*, 1988] model is commonly used for analytical modeling of stochastic unsaturated flow and transport [e.g., *Yeh et al.*, 1985a, 1985b; *Russo*, 1993, 1995; *Indelman et al.*, 1993; *Yang et al.*, 1996; *Zhang et al.*, 1998]. The *Gardner* [1958] model for unsaturated hydraulic conductivity is

$$K(\mathbf{x}) = K_s(\mathbf{x})\ \exp[-\alpha(\mathbf{x})h(\mathbf{x})] \tag{12}$$

where $\alpha(\mathbf{x})$ is the *Gardner* [1958] parameter defined as the slope of $\ln[K(\mathbf{x})]/h(\mathbf{x})$, and $K_s(\mathbf{x})$ is the saturated hydraulic conductivity. The *Russo* [1988] moisture content function is

$$\theta_e = (\theta_s - \theta_r)\{[1 + 0.5\alpha(\mathbf{x})h(\mathbf{x})]\exp[-0.5\alpha(\mathbf{x})h(\mathbf{x})]\}^{2/(m+2)} \tag{13}$$

where m is a parameter related to media tortuosity and θ_s is the saturated moisture content. We assume that $\alpha(\mathbf{x})$ and the log transform of the saturated hydraulic conductivity $f(\mathbf{x}) = \ln[K_s(\mathbf{x})]$ are normally distributed, second-order stationary random space functions, each consisting of a constant mean and a spatially varying perturbation: $f(\mathbf{x}) = \langle f\rangle + f'(\mathbf{x})$ and $\alpha(\mathbf{x}) = \langle\alpha\rangle + \alpha'(\mathbf{x})$. Our previous studies [*Holt*, 2000; *Holt et al.*, 2002] suggest that measurement errors can induce an apparent correlation between estimates of $\alpha(\mathbf{x})$ and $f(\mathbf{x})$ even when none exists. Nevertheless, we assume that the spatial covariance between $\alpha(\mathbf{x})$ and $f(\mathbf{x})$ is zero, because it is difficult to define a physically meaningful positive semidefinite cross-covariance function. The log transform of (12) is

$$Y(\mathbf{x}) = \langle F\rangle + f'(\mathbf{x}) - [\langle\alpha\rangle + \alpha'(\mathbf{x})][\langle h\rangle + h'(\mathbf{x})] \tag{14}$$

with, to the first order

$$\langle Y\rangle = \langle F\rangle - \langle\alpha\rangle\langle h\rangle \tag{15}$$

$$Y'(\mathbf{x}) = f'(\mathbf{x}) - \langle h\rangle\alpha'(\mathbf{x}) - \langle\alpha\rangle h'(\mathbf{x}) \tag{16}$$

$$\sigma^2_{Y'} = \sigma^2_f + \langle h\rangle^2\sigma^2_\alpha + \langle\alpha\rangle^2\sigma^2_h - 2\langle\alpha\rangle\sigma^2_{fh} + 2\langle h\rangle\langle\alpha\rangle\sigma^2_{\alpha h} \tag{17}$$

where σ^2_f is the variance of $\ln[K_s(\mathbf{x})]$, σ^2_α is the variance of $\alpha(\mathbf{x})$, σ^2_h is the tension head variance, σ^2_{fh} is the point covariance between $f(\mathbf{x})$ and $h(\mathbf{x})$, and $\sigma^2_{\alpha h}$ is the point covariance between $\alpha(\mathbf{x})$ and $h(\mathbf{x})$. In deriving (15), we assumed that $\sigma^2_{\alpha h}$ is small ($\ll$1). Because we assume that the hydraulic head is a stationary random process, the point covariance between the head perturbation and its gradient $\sigma^2_{hj_i}$ is identically equal to zero, and the point covariance between $Y'(\mathbf{x})$ and $j_i(\mathbf{x})$ is then

$$\sigma^2_{Y'j_i} = \sigma^2_{fj_i} - \langle h\rangle\sigma^2_{\alpha j_i} \tag{18}$$

where $\sigma^2_{fj_i}$ is the point covariance between $f(\mathbf{x})$ and $j_i(\mathbf{x})$ and $\sigma^2_{\alpha j_i}$ is the point covariance between $\alpha(\mathbf{x})$ and $j_i(\mathbf{x})$. The first-order mean, perturbation, and variance of the effective water content are [*Zhang et al.*, 1998]

$$\langle\theta_e\rangle = (\theta_s - \theta_r)\exp[-\langle\alpha\rangle\langle h\rangle/(m+2)][1 + 0.5\langle\alpha\rangle\langle h\rangle]^{2/(m+2)} \tag{19}$$

$$\theta_e'(\mathbf{x}) = \frac{\langle\theta_e\rangle}{(2 + \langle\alpha\rangle\langle h\rangle)(m+2)}\left(\langle\alpha\rangle\langle h\rangle^2\alpha'(\mathbf{x}) + \langle\alpha\rangle^2\langle h\rangle h'(\mathbf{x})\right) \tag{20}$$

$$\sigma^2_{\theta_e} = \frac{\langle\theta_e\rangle^2}{(2 + \langle\alpha\rangle\langle h\rangle)^2(m+2)^2} \cdot \left(\langle\alpha\rangle^2\langle h\rangle^4\sigma^2_\alpha + 2\langle\alpha\rangle^3\langle h\rangle^3\sigma^2_{\alpha h} + \langle\alpha\rangle^4\langle h\rangle^2\sigma^2_h\right) \tag{21}$$

The point covariance between q_i and θ_e is

$$\sigma^2_{q_i\theta_e} = \frac{\langle\theta_e\rangle K^G}{(2 + \langle\alpha\rangle\langle h\rangle)(m+2)} \cdot \begin{pmatrix} \delta_{i1}\langle\alpha\rangle^2\langle h\rangle\sigma^2_{fh} + \langle\alpha\rangle\langle h\rangle^2\sigma^2_{\alpha j_i} - 2\delta_{i1}\langle\alpha\rangle^2\langle h\rangle^2\sigma^2_{\alpha h} \\ -\delta_{i1}\langle\alpha\rangle\langle h\rangle^3\sigma^2_\alpha - \delta_{i1}\langle\alpha\rangle^3\langle h\rangle\sigma^2_h \end{pmatrix} \tag{22}$$

Table 1. Required Stochastic Functions for the Gardner–Russo Model

Statistic	3D isotropic[a]		1D/3D perfectly stratified[b]	
σ_h^2	$\frac{\sigma_f^2}{\langle\alpha\rangle^2}F_1(\lambda_f) + \frac{\langle h\rangle^2\sigma_\alpha^2}{\langle\alpha\rangle^2}F_1(\lambda_\alpha)$	(24)	$\frac{\sigma_f^2\lambda_f}{(1+\langle\alpha\rangle\lambda_f)\langle\alpha\rangle} + \frac{\langle h\rangle^2\sigma_\alpha^2\lambda_\alpha}{(1+\langle\alpha\rangle\lambda_\alpha)\langle\alpha\rangle}$	(25)
σ_{fh}^2	$\frac{\sigma_f^2}{\langle\alpha\rangle}F_1(\lambda_f)$	(26)	$\frac{\sigma_f^2\lambda_f}{(1+\langle\alpha\rangle\lambda_f)}$	(27)
$\sigma_{\alpha h}^2$	$-\frac{\langle h\rangle\sigma_\alpha^2}{\langle\alpha\rangle}F_1(\lambda_\alpha)$	(28)	$-\frac{\langle h\rangle\sigma_\alpha^2\lambda_\alpha}{(1+\langle\alpha\rangle\lambda_\alpha)}$	(29)
σ_{fj}^2	$-\frac{\langle h\rangle\sigma_\alpha^2}{\langle\alpha\rangle}F_2(\lambda_\alpha)$	(30)	$\frac{\sigma_f^2}{(1+\langle\alpha\rangle\lambda_f)}$	(31)
$\sigma_{\alpha j}^2$	$-\langle h\rangle\sigma_\alpha^2F_2(\lambda_\alpha)$	(32)	$-\frac{\langle h\rangle\sigma_\alpha^2}{(1+\langle\alpha\rangle\lambda_\alpha)}$	(33)
σ_j^2	$\sigma_f^2F_3(\lambda_f) + \langle h\rangle^2\sigma_\alpha^2F_3(\lambda_\alpha)$	(34)	**N/A**	
$F_1(\lambda_p)$[a]	$1 - \frac{2\ln(1+\langle\alpha\rangle\lambda_p)}{\langle\alpha\rangle\lambda_p} + \frac{1}{1+\langle\alpha\rangle\lambda_p}$			(35)
$F_2(\lambda_p)$[a]	$\frac{2}{\langle\alpha\rangle^2\lambda_p^2}\left[1 - \frac{2\ln(1+\langle\alpha\rangle\lambda_p)}{\langle\alpha\rangle\lambda_p} + \frac{1}{1+\langle\alpha\rangle\lambda_p}\right] - \frac{1}{1+\langle\alpha\rangle\lambda_p}$			(36)
$F_3(\lambda_p)$[a]	$\frac{1}{2\langle\alpha\rangle\lambda_p} - \frac{1}{\langle\alpha\rangle^2\lambda_p^2} + \frac{2}{\langle\alpha\rangle^3\lambda_p^3} - \frac{5}{\langle\alpha\rangle^4\lambda_p^4}$ $-\frac{1}{\langle\alpha\rangle^5\lambda_p^5}\left(\frac{\langle\alpha\rangle\lambda_p}{1+\langle\alpha\rangle\lambda_p} - 6\ln\lvert 1+\langle\alpha\rangle\lambda_p\rvert\right)$			(37)

[a] From the work of *Yeh et al.* [1985a, 1985b, 1985c].
[b] From the work of *Zhang et al.* [1998].

[11] We assume that the spatial structure of $f(\mathbf{x})$ and $\alpha(\mathbf{x})$ are both completely described by an exponential covariance function

$$C_p(\mathbf{r}) = \sigma_p^2 \exp\left(-\frac{|\mathbf{r}|}{\lambda_p}\right) \tag{23}$$

where $C_p(\mathbf{r})$ is the covariance function as a function of separation distance $\mathbf{r}$, σ_p^2 is the variance, and λ_p is the correlation length of parameter p. With this covariance function we are able to derive relationships for, σ_h^2, σ_{fh}^2, $\sigma_{\alpha h}^2$, $\sigma_{fj_i}^2$, $\sigma_{\alpha j_i}^2$, and $\sigma_{j_i}^2$ (Table 1 with (24)–(37)) and determine the ensemble mean and variance of the velocity, which can be related to contaminant transport times.

[12] The integral scale of the vertical velocity in the vertical direction is

$$I_{u_1} = \frac{1}{\sigma_{u_1}^2}\int_0^\infty C_{u_1}(\mathbf{r})\, d\mathbf{r} \tag{38}$$

where $C_{u_1}(\mathbf{r})$ is the vertical velocity covariance. Using *Zhang et al.*'s [1998, equation (61)] expression for $C_{u_1}(\mathbf{r})$ for (11), the integral scale for the velocity during 1D vertical flow can be shown to be

$$I_{u_1} = \frac{\langle u_1\rangle^2\langle\alpha\rangle^2\langle h\rangle^2\sigma_f^2\lambda_f}{(2+\langle\alpha\rangle\langle h\rangle)^2(m+2)\sigma_{u_1}^2} \tag{39}$$

The longitudinal macrodispersivity can be defined as

$$A_1 = \frac{1}{\langle u_1\rangle}\int_0^t C_{u_1}(\langle u_1\rangle t')dt' = \frac{1}{\langle u_1\rangle^2}\int_0^z C_{u_1}(r)dr \tag{40}$$

where $z = \langle u_1\rangle t$ is the mean travel distance of a solute plume. For very large mean travel distances ($z \to \infty$), A_1 approaches a constant value given by

$$A_1 = \frac{\sigma_{u_1}^2}{\langle u_1\rangle^2}I_{u_1} \tag{41}$$

3. Methods

[13] We employ a Monte Carlo approach to illustrate the impact of small simple property measurement errors on stochastic model predictions. We assume that Richard's equation (1) and (2) is valid. We also assume that (12) describes the unsaturated hydraulic conductivity, (13) describes the moisture-characteristic function, and the parameter m in (13) is known and equal to 0. We assume that log saturated hydraulic conductivity $f(\mathbf{x})$ and the exponential parameter $\alpha(\mathbf{x})$ are second-order stationary, isotropic Gaussian random fields completely described by (23). We generate 221 pairs of $f(\mathbf{x})$ and $\alpha(\mathbf{x})$, with cov[$f(\mathbf{x})$, $\alpha(\mathbf{x})$] = 0, and vary the means of $f(\mathbf{x})$ and $\alpha(\mathbf{x})$ between pairs. Each combined field of $f(\mathbf{x})$ and $\alpha(\mathbf{x})$ constitutes an artificial reality. At every spatial location in a reality, we simulate tension infiltrometer measurements in the presence of simple errors and reestimate $f(\mathbf{x})$ and $\alpha(\mathbf{x})$. We calculate the spatial statistics (mean, variance, and correlation length) for the estimated fields of $f(\mathbf{x})$ and $\alpha(\mathbf{x})$. These spatial statistics along with the true spatial statistics of the fields are used to determine error in the ensemble statistics of velocity and the macrodispersion coefficient. Relevant details are discussed below.

[14] For each Monte Carlo simulation, we generate over 262,000 parameter pairs (a 512 by 512 random field) of $f(\mathbf{x})$ and $\alpha(\mathbf{x})$, with a fixed mean and variance. The means of $f(\mathbf{x})$ and $\alpha(\mathbf{x})$ are varied between simulations, while the variance of $f(\mathbf{x})$ remains arbitrarily fixed at 1.0 and the coefficient of variation (CV) for $\alpha(\mathbf{x})$ is fixed at 0.1 to prevent negative values of $\alpha(\mathbf{x})$ in the generated field. Because the stochastic

models require a normal distribution for $\alpha(\mathbf{x})$, our treatment of $\alpha(\mathbf{x})$ differs from that of *Holt et al.* [2002] where $\alpha(\mathbf{x})$ was lognormally distributed with a variance of $\ln(\alpha)$ equal to 1.0. Mean values vary across a parameter space representative of poorly to well-sorted silty sand to very coarse sand. We vary the mean of $\alpha(\mathbf{x})$ from 10^{-4} cm^{-1} (poorly sorted) to 0.1 cm^{-1} (well sorted) and the geometric mean of the saturated hydraulic conductivity $K_s^G = \exp(\langle f(\mathbf{x})\rangle)$ from 10^{-5} cm/s (sandy silt) to 0.1 cm/s (coarse sand).

[15] Random fields are generated using the FFT method [e.g., *Robin et al.*, 1993]. We employ a 2D, isotropic, exponential variogram model

$$\gamma(\mathbf{r}) = \sigma^2\left[1 - \exp\left(-\frac{\mathbf{r}}{\lambda}\right)\right] \tag{42}$$

where σ^2 is the variance of the random process and λ is the correlation length. In stochastic models, it is often assumed that the correlation lengths of unsaturated parameters are the same [e.g., *Yeh et al.*, 1985a, 1985b, 1985c; *Mantoglou and Gelhar*, 1987a, 1987b], and for convenience, we set all correlation lengths equal to 10 length units (grid increments). Across our entire parameter space, we conduct $17 \times 13 = 221$ Monte Carlo simulations, in which the mean of $f(\mathbf{x})$ is incremented by steps of size 0.576 (17 values) and the mean of $\alpha(\mathbf{x})$ is multiplied by 1.78 between simulations (13 values).

[16] For the large domains used here, fields generated by the FFT method preserve the theoretical statistics (mean, variance, and correlation length) reported above. Field mean values differ by less than 1% from the theoretical mean values. On average, field variances and correlation lengths derived by fitting (42) differ from the theoretical values by 2% and 8% respectively. Pairs of $f(\mathbf{x})$ and $\alpha(\mathbf{x})$ fields have an average correlation coefficient of -0.018. It is important to note that the actual field statistics, not the theoretical values, are considered as "true" values for our error analysis.

[17] We simulate tension infiltrometer measurements in the presence of simple errors to provide estimates of $f(\mathbf{x})$ and $\alpha(\mathbf{x})$. Many workers have used the tension infiltrometer to estimate the spatial statistics of these parameters [e.g., *DOE*, 1993; *Mohanty et al.*, 1994; *Jarvis and Messing*, 1995; *Shouse and Mohanty*, 1998]. It is a simple device for applying a constant (negative) pressure boundary condition to unsaturated soil. The design and operation of the tension infiltrometer is described by *Ankeny et al.* [1988]. With knowledge of two applied pressures and corresponding observed steady state flux rates, parameters f and α can be estimated using the analytical approximation of *Wooding* [1968]. We assume that *Wooding*'s [1968] approximation is exact, and that subsample-scale heterogeneity does not affect tension infiltrometer measurements.

[18] In this illustration we limit the number of tension infiltrometer errors and consider only two error scenarios. In the first, pressure transducer errors (there are two transducers used to estimate the tension infiltrometer flux rate and one transducer used to estimate the applied pressure at the disk source) yield errors in observations of flux rates and applied pressures. The second scenario includes these two observation errors but adds an error in the contact between the disk and the medium. The procedures for reestimating $f(\mathbf{x})$ and $\alpha(\mathbf{x})$ for each of the error scenarios are summarized below, but the reader is referred to the work of *Holt et al.* [2002] for details.

[19] Using the tension infiltrometer, $f(\mathbf{x})$ and $\alpha(\mathbf{x})$ can be estimated from two observed steady state flux rates, $\hat{Q}_1$ and $\hat{Q}_2$, at the applied tensions $\hat{h}_1$ and $\hat{h}_2$. We assume that the tension values employed for each observation are estimated to be $\hat{h}_1 = 2.0$ cm and $\hat{h}_2 = 7.0$ cm (common values used in tension infiltrometer studies) and that $\hat{h} = h + \xi$, where ξ is a random error. The true tensions (h_n) are calculated by subtracting ξ from, $\hat{h}_n$ for $n = 1,2$. We assume tensions are determined from a pressure transducer at the disk source, and the value of ξ is determined by randomly sampling a mean-zero normal distribution with $\sigma_\xi^2 = 0.4$ cm^2 [*Holt et al.*, 2002]. Given h_n, α, and $K_s = \exp(f)$, we calculate the true flux from the tension infiltrometer using [*Wooding*, 1968]

$$Q_n = \frac{K_s}{\alpha} e^{-\alpha h_n}\left(\alpha + \frac{4}{\pi r_d}\right)\pi r_d^2 \tag{43}$$

where r_d is the radius of the disk and is equal to 10 cm. Once the true flux rate is determined, we calculate the estimated flux $\hat{Q}_n$ by adding a mean-zero, normally distributed error with $\sigma_Q^2 = 0.00165$ cm^6/s^2 [*Holt et al.*, 2002] (estimated σ_Q^2 from laboratory tension infiltrometer data presented by *Ankeny et al.* [1988]). Sampling locations where $\hat{Q}_1 \le \hat{Q}_2$ are discarded, as they would be in practice.

[20] When contact errors are considered, we assume that all contact error occurs at the outside of the disk, effectively reducing the disk radius. We also assume that contact errors only occur when measurements are made at the higher tension (h_2). $\hat{Q}_1$ is estimated using the procedure outlined above, while $\hat{Q}_2$ is estimated using the same variance for σ_Q^2 but is estimated using an altered disk radius $r_d^* = r_d\sqrt{1-g}$, where g is randomly sampled from a uniform distribution over 0.0 to 0.1. This means that the disk radius may be reduced from 10 cm to a minimum of $\sim$9.5 cm.

[21] Once the estimated tensions ($\hat{h}_1$ and $\hat{h}_2$) and steady state flux rates ($\hat{Q}_1$ and $\hat{Q}_2$) are determined, the relative permeability parameter, α, is then estimated with [*Reynolds and Elrick*, 1991]

$$\hat{\alpha} = \frac{\ln(\hat{Q}_1/\hat{Q}_2)}{\hat{h}_2 - \hat{h}_1} \tag{44}$$

and f is estimated with

$$\hat{f} = \ln\left(\frac{\hat{\alpha}\hat{Q}_1 e^{\hat{\alpha}\hat{h}_1}}{\hat{\alpha}\pi r_d^2 + 4r_d}\right) \tag{45}$$

This procedure is repeated for all points in a reality.

[22] The mean, variance, correlation length are determined for each of our 221 sets of true fields [$f(\mathbf{x})$ and $\alpha(\mathbf{x})$] and estimated fields [$\hat{f}(\mathbf{x})$ and $\hat{\alpha}(\mathbf{x})$]. Local variograms are calculated using the GSLIB subroutine gam2 [*Deutsch and Journel*, 1992]

$$\gamma(\mathbf{r}) = \frac{1}{2N(\mathbf{r})}\sum_{i=1}^{N(\mathbf{h})}[U(\mathbf{x}_i + \mathbf{r}) - U(\mathbf{x}_i)]^2 \tag{46}$$

where $N(\mathbf{r})$ is the number of samples in lag interval $\mathbf{r}$ and $U(\mathbf{x})$ is the random field. The variograms are fit, using a

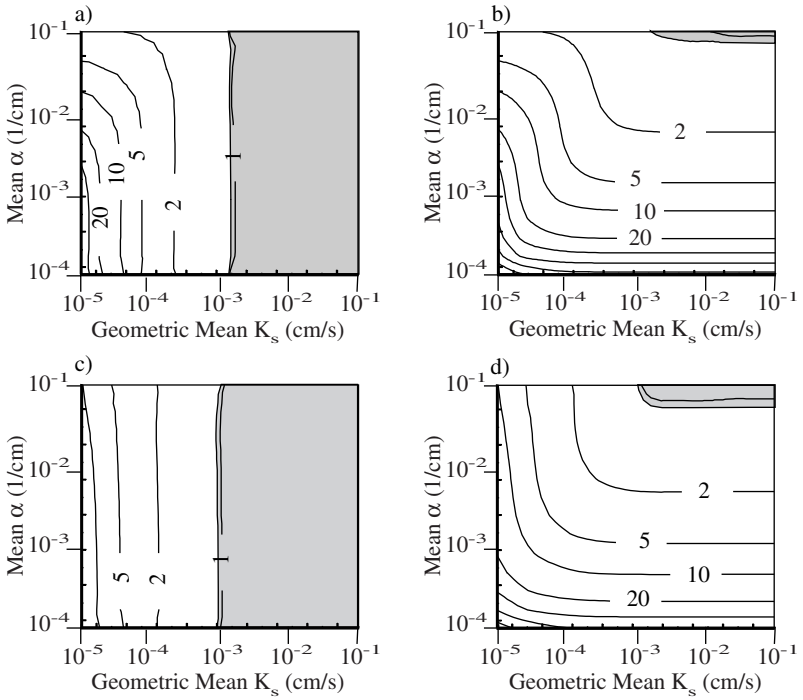

Figure 1. Upper figures: Parameter space plots of the ratio of the "estimated" to "true" geometric mean α for (a) observation scenario and (b) contact error scenario. Lower figures: ratio "estimated" to "true" geometric mean K_s for (c) observation scenario and (d) contact error scenario. Accurate regions ("estimated/true" between 0.95 and 1.05) are shaded. The horizontal axis represents grain size, from sandy silt on left to coarse sand on right. The vertical axis represents sorting, from poorly sorted at bottom to well sorted at top.

Levenberg–Marquardt algorithm, with the exponential variogram model

$$\gamma(\mathbf{r}) = \sigma^2\left[1 - \exp\left(-\frac{\mathbf{r}}{\lambda}\right)\right] + \sigma_n^2 \tag{47}$$

where λ is the estimated correlation length, σ^2 is the variance (referred to as the model variance by *Holt et al.* [2002]), and σ_n^2 is the nugget variance. Variogram fits are inspected to insure meaningful variogram model parameters. When a variogram is constant for all lag distances we refer to it as a "nugget variogram" in which $\sigma^2 = 0.0$ and $\lambda = 0.0$. Once these spatial statistics are determined, the mean and variance of the 3D and 1D velocity are calculated for all 221 sets of both the true and estimated fields using (9) and (11) and the appropriate subsidiary equations. Similarly, the 1D velocity integral scale and longitudinal macrodispersivity are determined from (39) and (41), respectively. Errors are quantified in contour maps of parameter space, using the ratio of the "estimated/true" value.

4. Errors in Spatial Statistics

[23] The stochastic models used in this illustrative study are parameterized with the spatial statistics for estimated log saturated conductivity $\hat{f}$ and the exponential parameter $\hat{\alpha}$. We first review the errors in these spatial statistics since they directly contribute to errors in stochastic model predictions. These errors differ from those presented by *Holt et al.* [2002]. Here we assume a normal distribution for $\alpha(\mathbf{x})$ with a CV fixed at 0.1, while *Holt et al.* [2002] assumed that $\alpha(\mathbf{x})$ was lognormally distributed, with a variance of 1.0. Their lognormal distribution translates to a $\text{var}[\alpha(\mathbf{x})] = 5 \times 10^{-8}$ cm^{-2}, at a geometric mean α of 10^{-4} cm^{-1}, and a $\text{var}[\alpha(\mathbf{x})] = 5 \times 10^{-2}$ cm^{-2}, at a geometric mean α of 0.1 cm^{-1}. In contrast, the normally distributed $\alpha(\mathbf{x})$ used here has a much smaller variance, ranging from 10^{-8} cm^{-2} at $\langle\alpha\rangle = 10^{-4}$ cm^{-1} to 10^{-4} cm^{-2} at $\langle\alpha\rangle = 0.1$ cm^{-1}.

[24] *Holt et al.* [2002] observed that both observation and contact errors lead to biased estimates of the exponential parameter $\langle\hat{\alpha}\rangle$ and log saturated conductivity $\langle\hat{f}\rangle$, which are overestimated, especially when the actual values of saturated conductivity $\langle f\rangle$ and $\langle\alpha\rangle$ are both small. Our results here are similar, as shown in the parameter space plots of error presented in Figure 1. The observation error scenario is on the left of the figure and the contact error scenario is on the right. Errors for $\langle\hat{\alpha}\rangle$ are plotted at the top and log saturated conductivity $\langle\hat{f}\rangle$ errors are at the bottom; the plots for the two parameters are similar for a given scenario. Keep in mind that these error plots are plots of the ratio of the "estimated" value divided by the "true" value. The bias is especially significant when the actual values of $\langle f\rangle$ and $\langle\alpha\rangle$ are both small (lower left corner of each figure), representing a poorly sorted sandy silt. For example, when estimating $\langle\hat{\alpha}\rangle$ errors in the log-flux ratio, $\ln(\hat{Q}_1/\hat{Q}_2)$ from (44), are higher for small $\langle\alpha\rangle$ and $\hat{Q}_1$ tends to be overestimated, while $\hat{Q}_2$ is underestimated at small $\langle f\rangle$. It is obvious from (44) that both of these conditions cause overestimation of $\hat{\alpha}$. When contact error is also present (Figure 1b), $\langle\hat{\alpha}\rangle$ is significantly overestimated at low $\langle\alpha\rangle$ for all values of

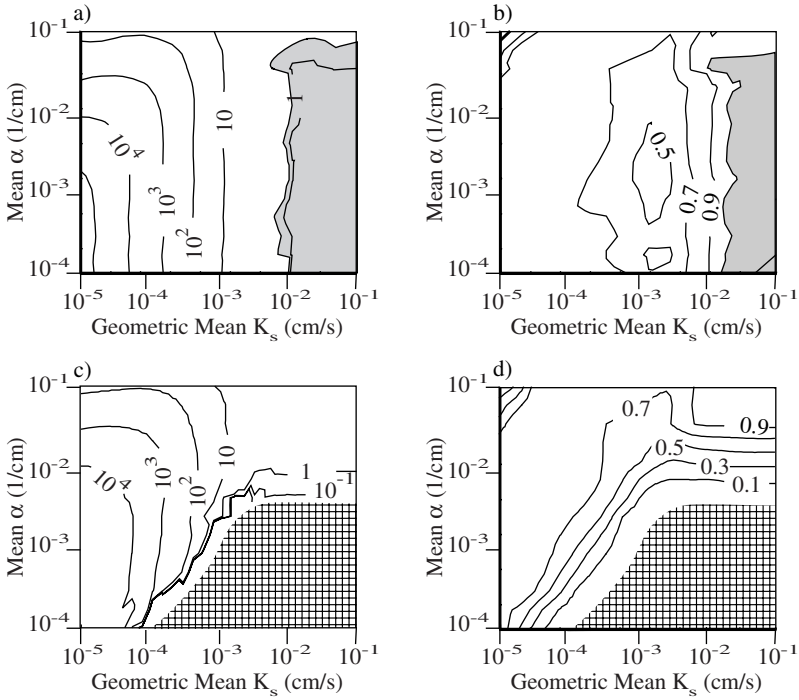

Figure 2. Ratio of the "estimated" to "true" variogram parameters for α. Observation error scenario: errors in (a) variance and (b) correlation length. Contact error scenario: errors in (c) variance and (d) correlation length. Accurate regions ("estimated/true" between 0.95 and 1.05) are shaded and regions where "estimated/true" = 0.0 are cross hatched. Note that (c) shows no shading of the accurate region for clarity, because the accurate region is small.

$\langle f \rangle$. Contact errors cause underestimation of $\hat{Q}_2$, leading to an increase in the log-flux ratio and erroneously high $\hat{\alpha}$. These effects are most pronounced at low $\langle \alpha \rangle$, where the true flux ratio tends to be very small.

[25] Errors in estimated log saturated conductivity $\langle \hat{f} \rangle$ increase at small $\langle f \rangle$, on the left side of the parameter space plots in Figures 1c and 1d. From (45) we can see that $\hat{f}$ is proportional to the log of both $\hat{Q}_1$ and $\hat{\alpha}$. These two parameters tend to be overestimated at small $\langle f \rangle$, causing overestimation of $\langle \hat{f} \rangle$. When the contact error is also present (Figure 1d), $\hat{\alpha}$ tends to be greatly overestimated at low $\langle \alpha \rangle$, leading to significant overestimation of $\langle \hat{f} \rangle$.

[26] Errors in the estimated variogram parameters bear less of a resemblance to those of the work of *Holt et al.* [2002]. The variance of the estimated exponential parameter $\hat{\alpha}$, or $\sigma^2_{\hat{\alpha}}$, follows a similar pattern to the published results and increases with decreasing $\langle f \rangle$ and $\langle \alpha \rangle$, as shown in the lower left corner of Figure 2a for the observation error scenario. However, the magnitude of the error metric in this plot is much greater than that published, because the variance of α is much smaller here and because the metric is a ratio and is divided by this small variance. Also in contrast to the published results, $\lambda_{\hat{\alpha}}$, the correlation length of $\hat{\alpha}$, tends to underestimate the correlation length of α (Figure 2b), because variability due to errors in $\hat{Q}_1$ and $\hat{Q}_2$ tends to mask the true spatial structure of α when σ^2_{α} is small. As $\langle f \rangle$ decreases these effects are more pronounced. When contact errors are also present, error in $\hat{Q}_2$ becomes independent of the sampled hydraulic properties, especially at low $\langle \alpha \rangle$. This effectively eliminates the spatial correlation of $\hat{\alpha}$, and the statistics $\sigma^2_{\hat{\alpha}}$ and $\lambda_{\hat{\alpha}}$ are greatly underestimated, especially in the lower right corner of parameter space (Figures 2c and 2d).

[27] Errors in the variance, $\sigma^2_{\hat{f}}$, of estimated log saturated conductivity, $\hat{f}$, and its correlation length, $\lambda_{\hat{f}}$ (Figure 3), are very similar to those of the work of *Holt et al.* [2002] if only observation errors are present (upper part of figure). When contact errors are present (lower part of figure), however, errors in $\sigma^2_{\hat{f}}$ are smaller than before because the variograms and cross-covariogram terms containing α contribute little to the estimated variance. In the study by *Holt et al.* [2002], these terms are much larger and cause significant overestimation of $\sigma^2_{\hat{f}}$.

5. Stochastic Model Errors

[28] In this section we present stochastic model predictions for both the observation and contact error scenarios. We first consider errors affecting predictions of the mean velocity $\langle \hat{u}_1 \rangle$. Because $\langle \hat{u}_1 \rangle$ is a first-order approximation it is the same for both the 3D isotropic and the 1D perfectly stratified cases. We then present the errors for the velocity variance $\sigma^2_{\hat{u}_1}$ that occur for each of these two cases. Finally, we present errors for the integral scale of the velocity I_{u_1} and for 1D large-scale, longitudinal macrodispersivity.

[29] The biased spatial statistics of $\hat{f}(\mathbf{x})$ and $\hat{\alpha}(\mathbf{x})$ lead to erroneous stochastic model predictions in two ways. First, statistical parameter errors also produce bias, or systematic distortion, in the model predictions. As with parameter errors, these prediction errors are depicted using contour maps of ratios; in this case they are ratios of the "esti-

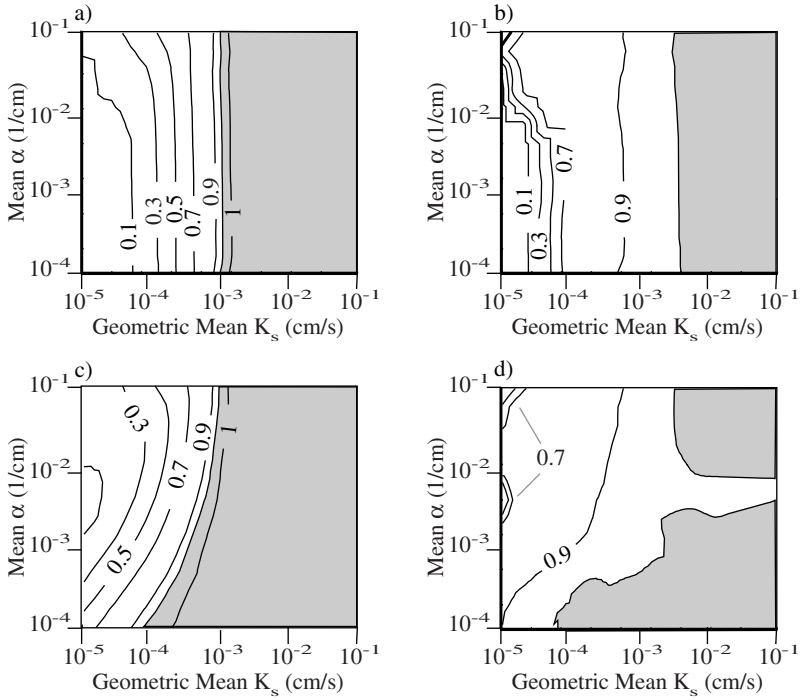

Figure 3. Ratio of the "estimated" to "true" variogram parameters for *f*. Observation error scenario: errors in (a) variance and (b) correlation length. Contact error scenario: errors in (c) variance and (d) correlation length. Accurate regions ("estimated/true" between 0.95 and 1.05) are shaded.

mated" prediction divided by the "true" prediction, plotted across the parameter space. Second, erroneous spatial statistics can cause some model assumptions to be violated. For the first-order models considered here the critical assumptions are that $\sigma^2_{\theta_e}/\langle\theta_e\rangle^2 \ll 1$, required for (9), and $\sigma^2_{\alpha h} \ll 1$, required for deriving (15). This last condition is more restrictive, and regions of the parameter space where $\sigma^2_{\hat{\theta}_e}/\langle\hat{\theta}_e\rangle^2 > 1$ are excluded from the plots. The excluded area increases with mean tension $\langle h\rangle$ and, in the contact error scenario, occupies the entire parameter space when tension reaches $\langle h\rangle = 1000$ cm. Consequently, the presented error plots are for selected mean tensions $\langle h\rangle$ of 10, 100, and 900 cm, representing wet to dry soils.

[30] Errors in the mean velocity due to observation errors are shown for the three different mean tensions $\langle h\rangle$ in Figure 4. Under very wet conditions (Figure 4a), $\langle\hat{u}_1\rangle$ is most sensitive to the geometric mean of saturated conductivity $\hat{K}_s$, and errors in the mean velocity mimic errors in $\langle\hat{f}\rangle$ (Figure 1c). As a result, $\langle\hat{u}_1\rangle$ is accurately estimated at large $\langle f\rangle$ (right side of parameter space) and is overestimated by more than a factor of 5 at small $\langle f\rangle$ (left side of parameter space). Some deviations occur at high $\langle\alpha\rangle$ (upper portion of parameter space), because overestimation of $\langle\hat{\alpha}\rangle$ leads to a reduction in $\langle\hat{u}_1\rangle$. At moderate tensions $\langle h\rangle$ (Figure 4b), errors in $\langle\hat{u}_1\rangle$ change significantly, and the excluded region, $\sigma^2_{\hat{\theta}_e}/\langle\hat{\theta}_e\rangle^2 > 1$, occupies roughly a third of the parameter space, concentrated in its upper left corner (e.g., representing well sorted, sandy silt). Along the boundary of the excluded region, overestimation of $\langle\hat{\alpha}\rangle$ leads to underprediction of $\langle\hat{u}_1\rangle$. In the lower left corner where $\langle f\rangle$ and $\langle\alpha\rangle$ are small, the mean velocity $\langle\hat{u}_1\rangle$ remains dominated by errors in the geometric mean $\hat{K}_s$ and is overestimated. At very high tension $\langle h\rangle$ (Figure 4c), the excluded region occupies most of the parameter space. For example, even without measurement error $\sigma^2_{\theta_e}/\langle\theta_e\rangle^2$ is greater than 1 for $\langle\alpha\rangle$ exceeding 0.02 cm^{-1}. Regardless of the value of tension $\langle h\rangle$, the mean velocity $\langle\hat{u}_1\rangle$ is accurately estimated at large log saturated conductivity $\langle f\rangle$, because $\langle\hat{\alpha}\rangle$ and $\langle\hat{f}\rangle$ are accurately estimated.

[31] When contact errors are also present the mean velocity $\langle\hat{u}_1\rangle$ errors have similar features (Figure 5). At low tension (Figure 5a) $\langle\hat{u}_1\rangle$ reflects the errors in $\langle\hat{f}\rangle$ (Figure 1c) and is overestimated by up to a factor 20. At progressively higher tension $\langle h\rangle$ (Figures 5b and 5c), the error decreases, and the narrow accurate region for $\langle\hat{u}_1\rangle$, defined by $\langle\hat{u}_1\rangle/\langle u_1\rangle$ between 0.95 and 1.05, sweeps across the parameter space. At very high tension $\langle h\rangle$ (Figure 5c), the mean velocity $\langle\hat{u}\rangle$ is always underestimated, because this narrow accurate region has passed out of the parameter space.

[32] Errors in the velocity variance, $\sigma^2_{\hat{u}_1}$, are shown for the observation error scenario in Figure 6 and for the contact error scenario in Figure 7. In these figures tension increases from top (wet) to bottom (dry). The 3D isotropic flow model is on the left, and the 1D model is on the right. At low tensions, errors in the velocity variance $\sigma^2_{\hat{u}_1}$ mimic errors in the mean velocity $\langle\hat{u}_1\rangle$. At higher tensions, the error pattern changes and becomes more complex, reflecting errors in the correlation lengths and variances of $\hat{\alpha}$ and $\hat{f}$. As $\langle\alpha\rangle$ increases and $\langle f\rangle$ decreases, toward the boundary of the feasible region, errors in $\sigma^2_{\hat{u}}$ increase, because the cross-covariance $\sigma^2_{\hat{q}\hat{\theta}_e}$ from (22) is overestimated due to errors in $\sigma^2_{\hat{\alpha}}$ and in the products of $\langle\hat{\alpha}\rangle$ and $\langle h\rangle$. In the observation error scenario (Figure 6), $\sigma^2_{\hat{u}_1}$ is accurately estimated in an irregular region in the lower right corner of the parameter space, where $\langle\alpha\rangle$ is small and $\langle f\rangle$ is large (poorly sorted

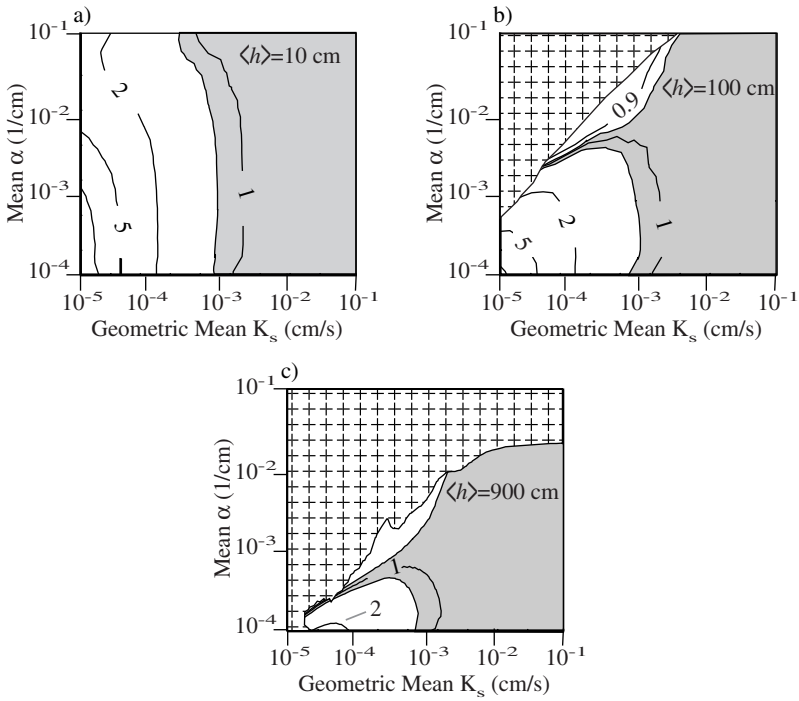

Figure 4. Ratio of the "estimated" to "true" mean velocity predicted using data from the observation error scenario. Results are shown for three different mean tensions $\langle h \rangle$ (values shown on graphs). Accurate regions ("estimated/true" between 0.95 and 1.05) are shaded, and regions where $\sigma^2_{\hat{\theta}_e} / \langle \hat{\theta}_e \rangle^2 > 1$ are patterned.

coarse sands), regardless of mean tension. In the contact error scenario (Figure 7), a narrow accurate region for $\sigma^2_{\hat{u}_1}$ sweeps across the parameter space as the mean tension increases.

[33] While the $\sigma^2_{\hat{u}_1}$ error patterns are the same for both the 3D and 1D cases, the magnitude of the errors are strikingly different (Figures 6 and 7). During 1D flow, $\sigma^2_{\hat{u}_1}$ error may be over four orders of magnitude larger than during 3D

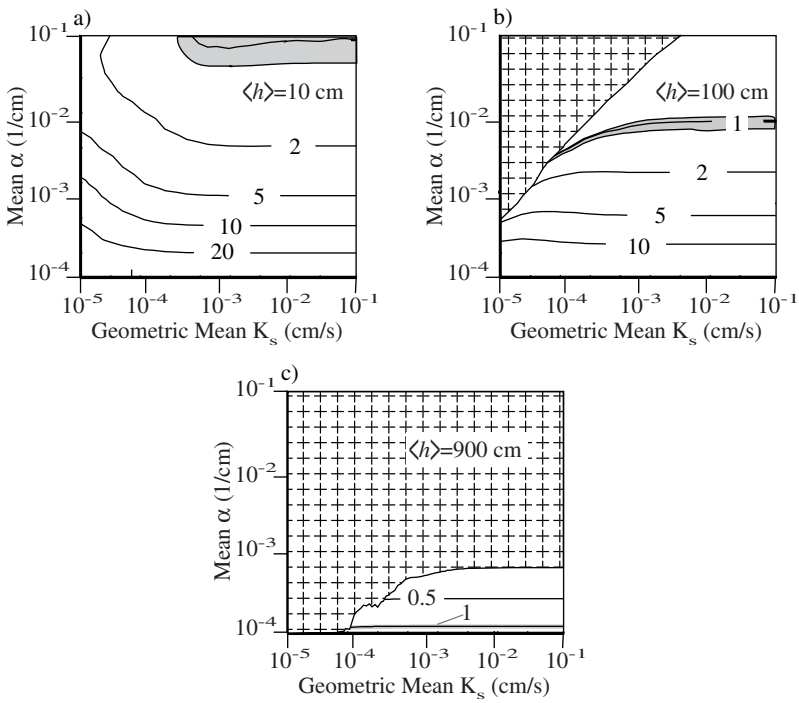

Figure 5. Ratio of the "estimated" to "true" mean velocity predicted using data from the contact error scenario. Results are shown for three different mean tensions $\langle h \rangle$ (values shown on graphs). Accurate regions ("estimated/true" between 0.95 and 1.05) are shaded, and regions where $\sigma^2_{\hat{\theta}_e} / \langle \hat{\theta}_e \rangle^2 > 1$ are patterned.

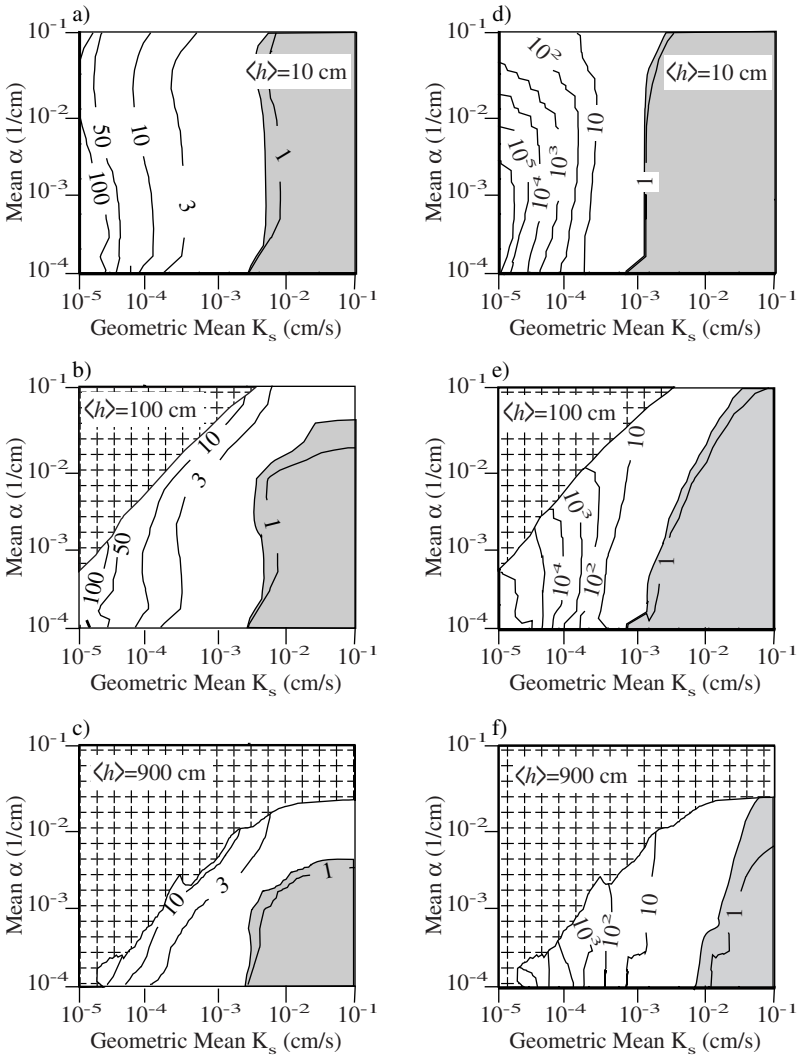

Figure 6. Ratio of the "estimated" to "true" velocity variance predicted using data from the observation error scenario. Results for 3D isotropic flow in (a)–(c) and 1D flow in (d)–(f). Results are shown for three different mean tensions $\langle h \rangle$ (values shown on graphs). Accurate regions ("estimated/true" between 0.95 and 1.05) are shaded, and regions where $\sigma^2_{\hat{\theta}_e} / \langle \theta_e \rangle^2 > 1$ are patterned.

flow. This result is not surprising, because measurement errors increase the apparent heterogeneity of $\hat{\alpha}$ and 1D flow samples all of the heterogeneity, while flow diverts around low permeability zones during 3D flow.

[34] Errors in the integral scale of the 1D velocity, I_{u_1}, are presented in Figure 8 and tend to be inversely proportional to errors in the velocity variance $\sigma^2_{\hat{u}_1}$. In the observation error scenario, I_{u_1} is accurately estimated in a small region in the lower right corner of parameter space, with low $\langle \alpha \rangle$ and $\langle f \rangle$ large, regardless of mean tension. In the contact error scenario, the velocity integral scale is never accurately estimated. The integral scale of velocity tends to be underestimated as mean tension increases, because the velocity is increasingly sensitive to errors in $\hat{\alpha}$.

[35] Errors in the 1D longitudinal macrodispersivity, A_1, are small (Figure 9), because of compensating errors in $\langle \hat{u}_1 \rangle$, $\sigma^2_{\hat{u}_1}$, and I_{u_1} (41). In the observation error scenario, A_1 is accurately estimated across nearly the entire parameter space. In the contact error scenario, however, A_1 slightly overestimated. These results suggest that the 1D macrodispersivity is a fairly robust ensemble statistic at large travel distances.

[36] These parameter space plots for different predictions share certain common features. When only observation errors are present, a "sweet spot" occurs in the lower right corner of the parameter space, for most predicted variables. Here the log saturated conductivity $\langle f \rangle$ is large and the exponential parameter is $\langle \alpha \rangle$ small, representing a poorly sorted coarse sand. Estimates of the spatial statistics for parameters $\hat{\alpha}$ and $\hat{f}$ are accurate, and ensemble model predictions remain accurate regardless of tension. When contact errors are present, however, the accurate regions for the spatial statistics of $\hat{\alpha}$ and $\hat{f}$ do not overlie one another in parameter space. As a result, no sweet spot occurs, and a narrow region of accurate ensemble predictions shifts through the parameter space as tension changes. In general, the sweet spot is largest for macrodispersivity A_1 because of compensating errors, followed by mean velocity $\langle \hat{u}_1 \rangle$ which depends only on $\langle \hat{\alpha} \rangle$ and $\langle \hat{f} \rangle$, and is smallest for the velocity variance $\sigma^2_{\hat{u}_1}$ and the velocity integral scale I_{u_1}

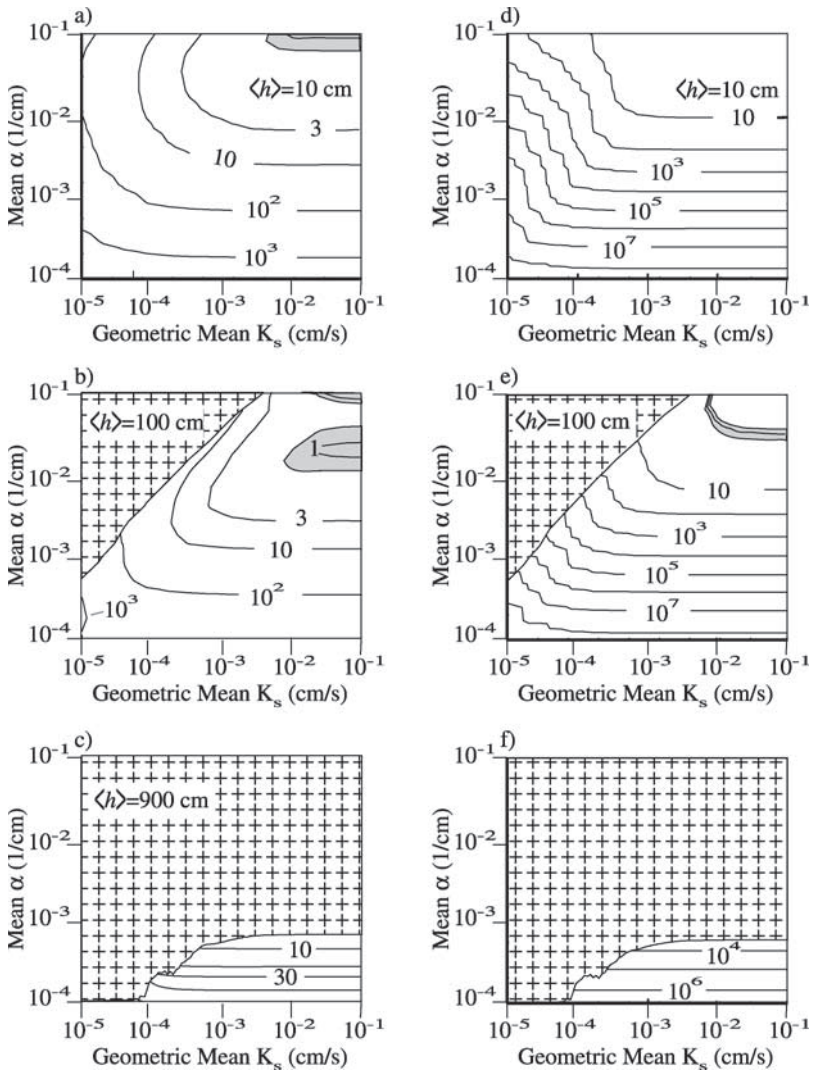

Figure 7. Ratio of the "estimated" to "true" velocity variance predicted using data from the contact error scenario. Results for 3D isotropic flow in (a)–(c) and 1D flow in (d)–(f). Results are shown for three different mean tensions $\langle h \rangle$ (values shown on graphs). Accurate regions ("estimated/true" between 0.95 and 1.05) are shaded, and regions where $\sigma^2_{\hat{\theta}_e} / \langle \hat{\theta}_e \rangle^2 > 1$ are patterned.

which depends on the variance and correlation lengths of $\hat{a}$ and $\hat{f}$.

6. Neglected Errors

[37] In this illustrative example we include only very small and simple forms of error and neglect many other types of error likely to affect tension infiltrometer measurements. In the work of *Holt et al.* [2002], we explained that actual tension infiltrometer flux rate errors are likely to be higher than those considered here. In tension infiltrometer reproducibility studies, *Holt et al.* [2002] found that $\sigma^2_Q = 0.06$ cm^6/s^2, more than an order of magnitude larger than the value $\sigma^2_Q = 0.00165$ cm^6/s^2 used here. In addition, errors in applied tension at the disk source may be much larger than considered here, because many tension infiltrometers do not use transducers in the base plate. We have also assumed that tension infiltrometer flux rates have truly reached steady state. In the field, however, it is nearly impossible to reach true steady state [*Logsdon*, 1997].

[38] We also considered a simple inversion-model error caused by poor contact between the tension infiltrometer and the sampled medium. Other types of inversion-model error, however, may be difficult to quantify or treat. These errors may include subsample heterogeneity, viscosity changes during infiltration, nonuniform wetting phase structure introduced by subsample scale heterogeneity or air entrapment, and incorrect parametric models for relative permeability.

[39] Given the wide range of types of error that may affect field measurements of unsaturated hydraulic properties, it may be impossible to model all errors that affect field measurements of unsaturated hydraulic properties. Consequently it may not be possible to use error analysis to determine suitable parameter spaces for a particular field device or to remove bias from estimated spatial statistics. This suggests that stochastic models based on these kinds of measurements might be too uncertain for use in decision-making processes.

[40] In this study we use every point in a reality to estimate spatial statistics. However, it is not possible to

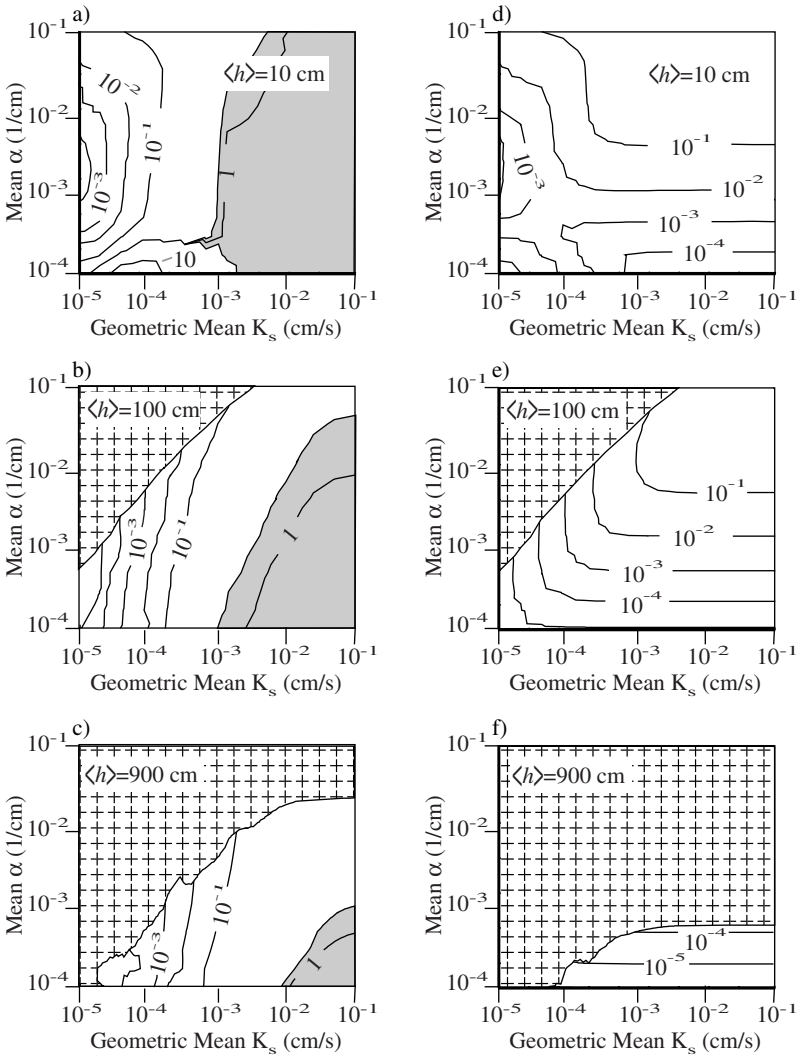

Figure 8. Ratio of the "estimated" to "true" 1D integral scale of the velocity predicted using data from the observation error scenario [(a)–(c)] and the contact error scenario [(d)–(f)]. Results are shown for three different mean tensions $\langle h \rangle$ (values shown on graphs). Accurate regions ("estimated/true" between 0.95 and 1.05) are shaded, and regions where $\sigma^2_{\hat{\theta}_e} / \langle \hat{\theta}_e \rangle^2 > 1$ are patterned.

sample everywhere, and estimates of spatial statistics are uncertain because of incomplete sampling and nonideal sample locations (structural errors). When measurement errors are present, structural errors increase significantly and the additional uncertainty can preclude reliable estimation of spatial statistics [*Holt*, 2000].

7. Summary and Implications

[41] We use Monte Carlo error analyses to illustrate the impact of hydraulic property measurement errors on stochastic model predictions. We construct a series of idealized artificial realities (spatially correlated random fields) completely described by the Gardner–Russo parametric model [*Gardner*, 1958; *Russo*, 1988]. Means of the parameters $\alpha(\mathbf{x})$ and $f(\mathbf{x}) = \ln[K_s(\mathbf{x})]$ are varied between 221 different realities to reveal the connection between true property values and prediction errors. Properties are estimated using simulated tension infiltrometer measurements subject to only small simple errors. We consider two error scenarios selected to show how different types of error affect stochastic model predictions. The first is an observation error scenario with only errors in estimates of tension infiltrometer flux rates and applied pressures at the disk source. The second is a contact error scenario that includes a boundary condition error due to poor contact between the tension infiltrometer disk and the sampled medium. The spatial statistics (mean, correlation length, and variance) for both the true and estimated parameter fields are determined using all locations within each reality to insure that model prediction errors reflect only errors in property measurements. Extensions of the unconditional stochastic flow and transport models of *Yeh et al.* [1985a, 1985b] (3D statistically isotropic) and of *Zhang et al.* [1998] (1D perfectly layered) are used to predict the ensemble mean, variance, and integral scale of velocity and the longitudinal macrodispersivity. Errors are quantified using the ratio of the "estimate" to the "true" value.

[42] Although the general trends are similar, errors in the parameter spatial statistics differ from the results presented

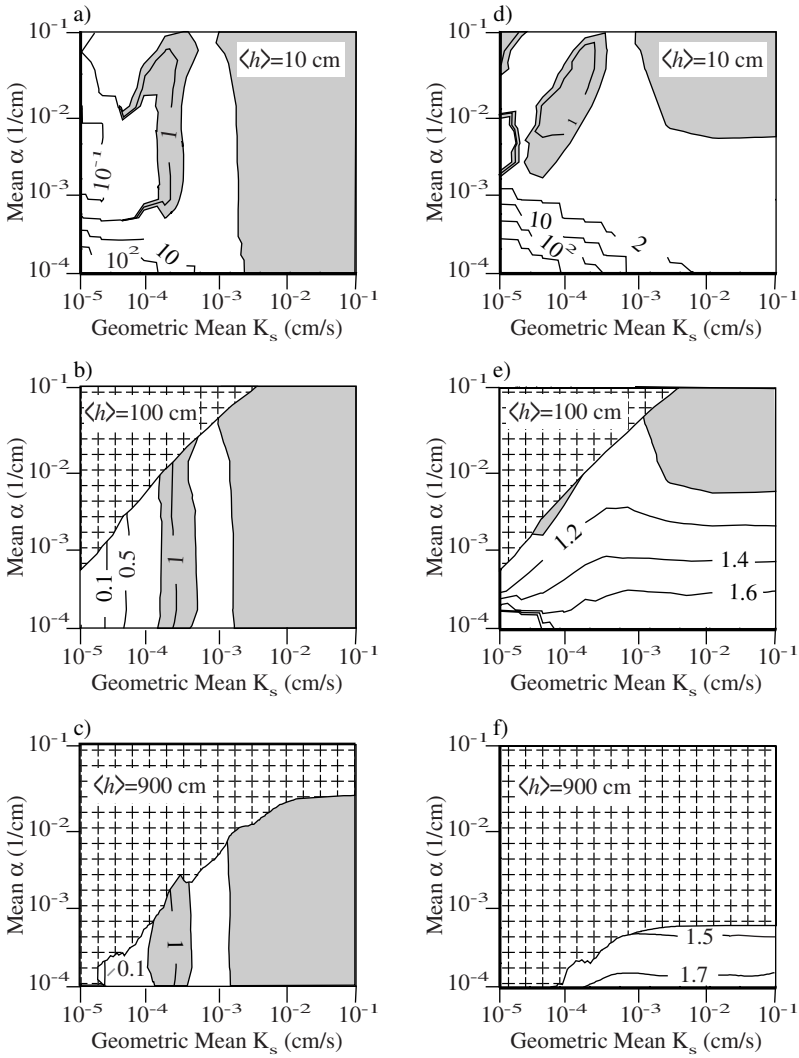

Figure 9. Ratio of the "estimated" to "true" longitudinal macrodispersivity (1D flow) predicted using data from the observation error scenario [(a)–(c)] and the contact error scenario [(d)–(f)]. Results are shown for three different mean tensions $\langle h \rangle$ (values shown on graphs). Accurate regions ("estimated/true" between 0.95 and 1.05) are shaded, and regions where $\sigma^2_{\hat{\theta}_e} / \langle \theta_e \rangle^2 > 1$ are patterned.

by *Holt et al.* [2002]. Major differences reflect the smaller variance of α due to our assumption here of a normal distribution for α, with fixed CV = 0.1. Because the spatial structure of $\hat{\alpha}$ is less varied, it is easily obscured by measurement errors, resulting in larger errors in the variance and under estimates of correlation length. In addition, variogram and cross-variogram terms containing α are smaller, leading to less error in $\sigma^2_{\hat{f}}$ when contact errors are present.

[43] The errors in the spatial statistics of parameters $\hat{f}(\mathbf{x})$ and $\hat{\alpha}(\mathbf{x})$ cause prediction errors for stochastic flow and transport models in two ways: (1) critical model assumptions may be violated, limiting the parameter space usable in the model and (2) model predictions become biased or systematically distorted. In our study, the assumption required for the first order approximations, $\sigma^2_{\hat{\theta}_e} / \langle \theta_e \rangle^2 \ll 1$, is violated across roughly a third of the parameter space in moderately dry conditions ($\langle h \rangle$ = 100 cm), and across more than one half of the parameter space under very dry conditions ($\langle h \rangle$ = 900 cm). When the mean tension is sufficiently high, e.g., $\langle h \rangle$ = 1000 cm, and contact errors are present, the assumption is violated across the entire parameter space.

[44] Where critical assumptions are valid stochastic model predictions still show significant error. The magnitude and pattern of error changes with mean tension. Mean velocities may be overestimated (wet conditions) or underestimated (dry conditions) by roughly an order of magnitude. Errors in velocity variances change with the dimensionality of flow, and the magnitude of the error decreases with mean tension. Errors are generally much worse for 1D stochastic flow, because all heterogeneity is sampled. The velocity variance is overestimated by up to three orders of magnitude during 3D flow and eight orders of magnitude during 1D flow. The 1D velocity integral scale varies as the inverse of the velocity variance. Consequently, it is generally underestimated by as much as five orders of magnitude. The estimate of the 1D longitudinal macrodispersivity is surprisingly robust. It generally shows relatively small error across most of the parameter space.

[45] When only observation errors occur a sweet spot develops in parameter space coincident with poorly sorted, coarse sand (low α and large K_s). In the sweet spot, all stochastic model predictions are accurate, because the spatial statistics of $\hat{f}(\mathbf{x})$ and $\hat{\alpha}(\mathbf{x})$ are accurate. When contact errors are present, no sweet spot develops, because the accurate regions for the spatial statistics of $\hat{f}(\mathbf{x})$ and $\hat{\alpha}(\mathbf{x})$ do not overlap.

[46] Our results suggest that property measurement errors can significantly impact stochastic model predictions and, by implication, the decisions based on those predictions. If property measurement errors are known and can be quantified, as in our case, it is possible to remove the effects of these errors. Unfortunately, it is impossible to explicitly know all errors *a priori*, and the number and potential effect of measurement errors is great. The consequences of unknown property errors are potentially severe. For the error scenarios considered here, one could unknowingly underpredict mean travel times by over an order of magnitude under wet conditions and overestimate travel times by nearly an order of magnitude under drier conditions.

[47] Our results also illustrate an important limitation of stochastic models. If input spatial statistics are not accurate, the magnitude of stochastic model errors changes with flow conditions. A sweet spot occurs only in that part of the parameter space where all input spatial statistics are accurately estimated. When measurements are affected only by observation errors, it is more likely that a sweet spot will develop in some part of a parameter space. When inversion-model errors affect measurements, it is less likely that the spatial statistics will be accurately estimated in an overlapping portion of the parameter space, and there will be no sweet spot. Similar behavior is likely when multiple properties are estimated from different methods, with varying measurement support, or at dissimilar timescales.

[48] Most practical applications of stochastic models involve conditioning on site-specific data and the use of boundary conditions and parameter fields that produce nonstationary flow conditions. When used in a decision-making process these models offer an advantage, because solutions are constrained by site-specific data and estimated second and higher moments are smaller, implying lower uncertainty and increased confidence in the results. When the hydraulic property data have been estimated in the presence of observation or inversion-model errors, however, the increased confidence may not be warranted, as bias in the results may erode the advantages of conditional approaches. This issue should be the subject of future research.

[49] **Acknowledgments.** This research was supported by the Department of Energy's Environmental Management Science Program (EMSP) through grant no. DE-FG07-96ER14704. We also thank Sean McKenna and Jan Hendrickx for their reviews of an earlier version of this manuscript. We are especially grateful to Allan Gutjahr for his contributions to the beginnings of this work and reviews of an early version of this manuscript. Finally, we appreciate the thoughtful comments of two anonymous reviewers; their efforts improved this manuscript.

References

Ankeny, M. D., T. C. Kaspar, and R. Horton, Design for an automated tension infiltrometer, *Soil Sci. Soc. Am. J.*, *52*, 893–896, 1988.

Deutsch, C. V., and A. G. Journel, *GSLIB: Geostatistical Software Library and User's Guide*, 2nd ed., Oxford Univ. Press, New York, 1992.

DOE, Hydrogeologic data for existing excavations at the Area 5 Radioactive Waste Management site, Nevada Test Site, Nye County, Nevada, *DOE/NV/11432-40*, U.S. Dept. of Energy, Nev. Oper. Off., Las Vegas, Nev., 1993.

Gardner, W. R., Some steady state solutions of unsaturated moisture flow equations with application to evaporation for a water table, *Soil Sci.*, *85*, 228–232, 1958.

Harter, T., and T.-C. J. Yeh, Stochastic analysis of solute transport in heterogeneous, variably saturated soils, *Water Resour. Res.*, *32*(6), 1585–1595, 1996.

Holt, R. M., *Spatial bias in unsaturated hydraulic property estimates: Origin, impact, and relevance*, Ph.D. Thesis, 160 pp., N. M. Inst. of Min. and Technol., Socorro, N. M., 2000.

Holt, R. M., J. L. Wilson, and R. J. Glass, Spatial bias in field-estimated unsaturated hydraulic properties, *Water Resour. Res.*, *38*(12), 1311, doi:10.1029/2002WR001336, in press, 2002.

Indelman, P., D. Or, and Y. Rubin, Stochastic analysis of unsaturated steady state flow through bounded heterogeneous formations, *Water Resour. Res.*, *29*(4), 1141–1148, 1993.

Jarvis, N. J., and I. Messing, Near-saturated hydraulic conductivity in soils of contrasting texture measured by tension infiltrometers, *Soil Sci. Soc. Am. J.*, *59*, 27–34, 1995.

Logsdon, S. D., Transient variation in the infiltration rate during measurement with tension infiltrometers, *Soil Sci.*, *162*, 233–241, 1997.

Mantoglou, A., and L. W. Gelhar, Capillary tension head variance, mean soil moisture content, and effective specific soil moisture capacity of transient unsaturated flow in stratified soils, *Water Resour. Res.*, *23*(1), 47–56, 1987a.

Mantoglou, A., and L. W. Gelhar, Effective hydraulic conductivities of transient unsaturated flow in stratified soils, *Water Resour. Res.*, *23*(1), 57–67, 1987b.

Mohanty, B. P., M. D. Ankeny, R. Horton, and R. S. Kanwar, Spatial analysis of hydraulic conductivity measured using disc infiltrometers, *Water Resour. Res.*, *30*(9), 2489–2498, 1994.

Reynolds, W. D., and D. W. Elrick, Determination of hydraulic conductivity using a tension infiltrometer, *Soil Sci. Soc. Am. J.*, *55*, 633–639, 1991.

Robin, M. J. L., A. L. Gutjahr, E. A. Sudicky, and J. L. Wilson, Cross-correlated random field generation with the direct Fourier transform method, *Water Resour. Res.*, *29*(7), 2385–2397, 1993.

Russo, D., Determining soil hydraulic properties by parameter estimation: On the selection of a model for the hydraulic properties, *Water Resour. Res.*, *24*(3), 453–459, 1988.

Russo, D., Stochastic modeling of macrodispersion for solute transport in heterogeneous unsaturated porous formations, *Water Resour. Res.*, *29*(2), 383–397, 1993.

Russo, D., Stochastic analysis of the velocity covariance and the displacement covariance tensors in partially saturated heterogeneous anisotropic porous formations, *Water Resour. Res.*, *31*(7), 1647–1658, 1995.

Shouse, P. J., and B. P. Mohanty, Scaling of near-saturated hydraulic conductivity measured using disc infiltrometers, *Water Resour. Res.*, *34*(5), 1195–1205, 1998.

Wooding, R. A., Steady infiltration from a shallow circular pond, *Water Resour. Res.*, *4*(6), 1259–1273, 1968.

Yang, J., R. Zhang, and J. Wu, An analytical solution of macrodispersivity for adsorbing solute transport in unsaturated soils, *Water Resour. Res.*, *32*(2), 355–362, 1996.

Yeh, T.-C. J., L. W. Gelhar, and A. L. Gutjahr, Stochastic analysis of unsaturated flow in heterogeneous soils, 1, Statistically isotropic media, *Water Resour. Res.*, *21*(4), 447–456, 1985a.

Yeh, T.-C. J., L. W. Gelhar, and A. L. Gutjahr, Stochastic analysis of unsaturated flow in heterogeneous soils, 2, Statistically isotropic media with variable α, *Water Resour. Res.*, *21*(4), 457–464, 1985b.

Yeh, T.-C. J., L. W. Gelhar, and A. L. Gutjahr, Stochastic analysis of unsaturated flow in heterogeneous soils, 3, Observations and applications, *Water Resour. Res.*, *21*(4), 465–471, 1985c.

Zhang, D. Z., T. C. Wallstrom, and C. L. Winter, Stochastic analysis of steady-state unsaturated flow in heterogeneous media: Comparison of the Brooks–Corey and Gardner–Russo models, *Water Resour. Res.*, *34*(6), 1437–1449, 1998.

R. J. Glass, Flow Visualization and Processes Laboratory, Sandia National Laboratories, Albuquerque, NM, USA.

R. M. Holt, Department of Geology and Geological Engineering, University of Mississippi, University, MS, USA. (rmholt@olemiss.edu)

J. L. Wilson, Department of Earth and Environmental Science, New Mexico Institute of Mining and Technology, Socorro, NM, USA.